# Supplementary Information

## Supplementary Table 1. Experimental protocol for aptamer selection by SELEX.

| Cycle | PAL [pmol] | Salmon Sperm DNA [mg $mL^{-1}$] | Heparin [mg $mL^{-1}$] | Trans-cription [µL] | Incubation Time [min] | Washing | Dark Elution Time [min] | PCR cycles |
|---|---|---|---|---|---|---|---|---|
| 1 | 125 | 0.08 | - | 20 | 30 | 1x short, 1x 3min | 30 | 10 |
| 2 | 125 | 0.08 | - | 20 | 30 | 1x short, 1x 3min | 30 | 9 |
| 3 | 125 | 0.08 | - | 20 | 30 | 1x short, 2x 3min | 30 | 10 |
| 4 | 125 | 0.08 | - | 20 | 30 | 1x short, 2x 3min | 30 | 8 |
| 5 | 125 | 0.08 | - | 20 | 30 | 1x short, 3x 3min | 30 | 8 |
| 6 | 125 | 0.08 | - | 20 | 30 | 6x short, 6x 3min | 30 | 8 |
| 7 | 125 | 0.08 | - | 20 | 30 | 7x short, 7x 3min | 25 | 7 |
| 8 | 125 | 0.08 | - | 20 | 30 | 8x short, 8x 3min | 20 | 7 |
| 9 | 125 | 0.08 | - | 20 | 30 | 9x short, 9x 3min | 15 | 7 |
| 10 | 75 | 0.1 | - | 20 | 30 | 1x short, 3x 15min | 15 | 10 |
| 11 | 15 | 0.5 | 1 | 20 | 20 | 1x short, 3x 15min | 15 | 14 |
| 12 | 3 | 0.5 | 1 | 20 | 10 | 1x short, 4x 15min | 15 | 17 |
| 13 | 3 | 0.5 | 1 | 5 | 5 | 1x short, 4x 15min | 15 | 17 |
| 14 | 0.3 | 1 | 2 | 5 | 3 | 1x short, 4x 15min | 15 | 19 |
| 15 | 0.03 | 1 | 4 | 5 | 1 | 1x short, 4x 15min | 15 | 19 |

**Supplementary Table 2. PAL crystallization - data collection and refinement statistics**

| | Native[a] | PAL SeMet[a] |
|---|---|---|
| **Data collection** | | |
| Space group | P 21 21 21 | P 21 21 21 |
| Cell dimensions | | |
| *a*, *b*, *c* (Å) | 67.01, 150.34, 219.78 | 66.96, 150.49, 219.64 |
| α, β, γ (°) | 90, 90, 90 | 90, 90, 90 |
| Resolution (Å) | 71.13 – 2.51 (2.60 – 2.51)[b] | 49.41 – 3.30 (3.39 – 3.30) |
| $R_{meas}$ | 0.228 (2.321) | 0.234 (1.37) |
| $I$ / σ$I$ | 8.00 (0.41) | 14.61 (1.7) |
| Completeness (%) | 98.7 (99.0) | 100 (99.9) |
| Redundancy | 4.3 (4.4) | 25.8 (10.9) |
| $CC_{1/2}$ | 0.930 (0.355) | 0.998 (0.663) |
| **Refinement** | | |
| Resolution (Å) | 71.13 – 2.51 (2.54 – 2.51) | |
| No. reflections | 76,052 (7,490) | |
| $R_{work}$ / $R_{free}$ | 0.243 (0.421) / 0.254 (0.425) | |
| No. atoms | | |
| Protein | 10,733 | |
| Ligand/ion | 155 | |
| Water | 158 | |
| *B*-factors | | |
| Protein | 80.47 | |
| Ligand/ion | 67.95 | |
| Water | 61.76 | |
| R.m.s deviations | | |
| Bond lengths (Å) | 0.004 | |
| Bond angles (°) | 1.01 | |

[a] Native and SAD data were collected from a single crystal each.

[b] Values in parentheses are for highest-resolution shell.

**Supplementary Table 3. Stabilities of aptamer hairpins and 5'UTRs predicted by Mfold[27].**

| | hairpin [kcal mol$^{-1}$] | 5'UTR [kcal mol$^{-1}$] |
|---|---|---|
| UTR1 | -30.1 | -36 |
| UTR2 | -30.1 | -36.3 to -37.1 |
| UTR3 | -30.1 | -34.9 |
| UTR4 | -30.1 | -35.9 |
| UTR5 | -30.1 | -36.5 to -37.7 |
| UTR6 | -17.2 | -23.8 |
| UTR7 | -17.2 | -22.8 |
| UTR8 | -17.2 | -24 to -25.2 |
| UTR9 | -22.2 | -28.8 |
| UTR10 | -22.2 | -27.6 |
| UTR11 | -22.2 | -29 to -30.2 |
| UTR12 | -28 | -34.6 |
| UTR13 | -28 | -33.4 |
| UTR14 | -28 | -34.8 to -36 |
| UTR15 | -36.2 | -43.1 to -44.3 |
| UTRdi | -17.7/-23 | -44.5 |
| UTRa5 | -30.5 | -36.9 to -38.1 |
| UTRa8 | -17.6 | -24.4 to -25.6 |

**Supplementary Table 4. PAL crystallization - pairwise refinement.**

| | model 2.51 Å [a] | model 2.67 Å | model 2.83 Å |
|---|---|---|---|
| $R_{work}$ (up to 2.83 Å) [b] | 0.2284 | 0.2268 | 0.2255 |
| $R_{free}$ (up to 2.83 Å) [c] | 0.2418 | 0.2441 | 0.2447 |
| $R_{free}$ (2.93 - 2.83 Å) [d] | 0.3477 | 0.3499 | 0.3607 |

[a] Resolution limit for diffraction data included in pairwise refinement.

[b] $R_{work}$ calculated up to a high-resolution limit of 2.83 Å.

[c] $R_{free}$ calculated up to a high-resolution limit of 2.83 Å.

[d] $R_{free}$ calculated for the highest-resolution shell from 2.93 to 2.83 Å.

**Supplementary Figure 1**


Multiple sequence alignment between PAL from *N. multipartita*, denoted *Nm*PAL (Genbank identifier 258557706), and two homologs from *N.* sp. 12Sc4-1, denoted *Ns*PAL1 and *Ns*PAL2 (1409114985 and 1409114630). Circles above the alignment denote secondary structure with α helices in tan, β sheets in blue and loop/unstructured regions in white. The asterisks below the alignment denote residues fully conserved between the three proteins.

**Supplementary Figure 2**

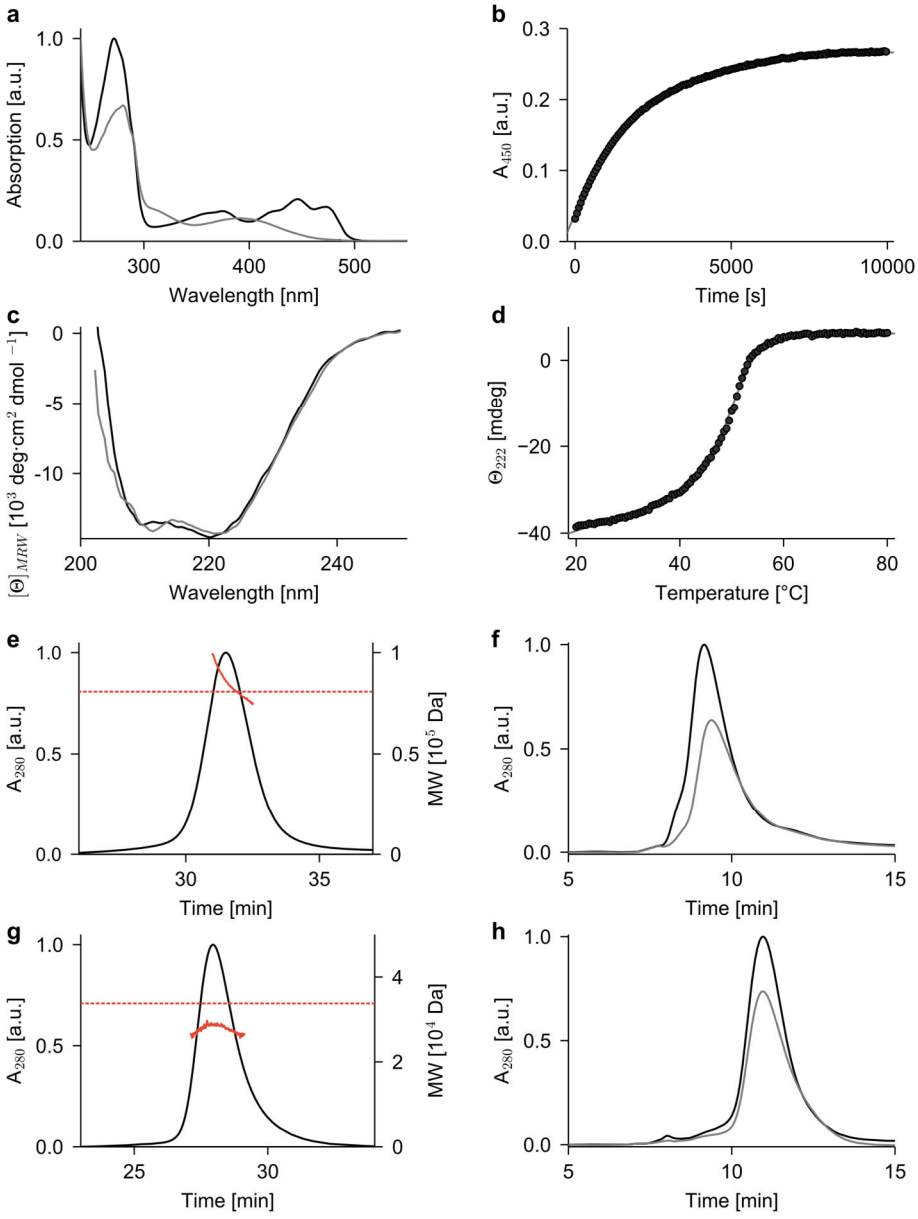


Biochemical and spectroscopic characterization of PAL. **a**, Steady-state UV-vis absorption spectra of PAL before (black) and immediately after blue-light exposure. The dark-adapted state $PAL_D$ shows characteristic three-pronged absorption around 450 nm, and the light-adapted state $PAL_L$ has an absorption maximum at 390 nm. **b**, Thermal recovery of PAL after blue-light exposure monitored by absorption at 450 nm. The dark-adapted form $PAL_D$ recovers

monoexponentially with a time constant of (2200 ± 50) s at 22°C. **c**, Circular dichroism (CD) measurements show little changes between $PAL_D$ and $PAL_L$ (black and grey lines). **d**, The midpoint of temperature-induced unfolding of PAL as monitored by CD spectroscopy amounts to $T_m$ = (50.2 ± 0.1) °C. All spectroscopic measurements were replicated at least twice with similar results. **e**, Size-exclusion chromatography (SEC) on a Superose 6 column coupled with multi-angle light scattering (MALS) reveals that dark-adapted PAL adopts homodimeric structure in solution. **f**, The SEC analysis of dark- and light-adapted PAL (black and grey lines) yields very similar retention times on a Superdex 75 column, thus indicating that the homodimeric receptor does not dissociate upon light absorption. **g**, SEC-MALS on a Superdex 75 column analysis of the isolated LOV domain of PAL reveals homodimeric state. **h**, SEC analysis on a Superdex 75 column indicates that the homodimeric state of PAL-LOV in the dark (black) is maintained under blue light (grey).

**Supplementary Figure 3**

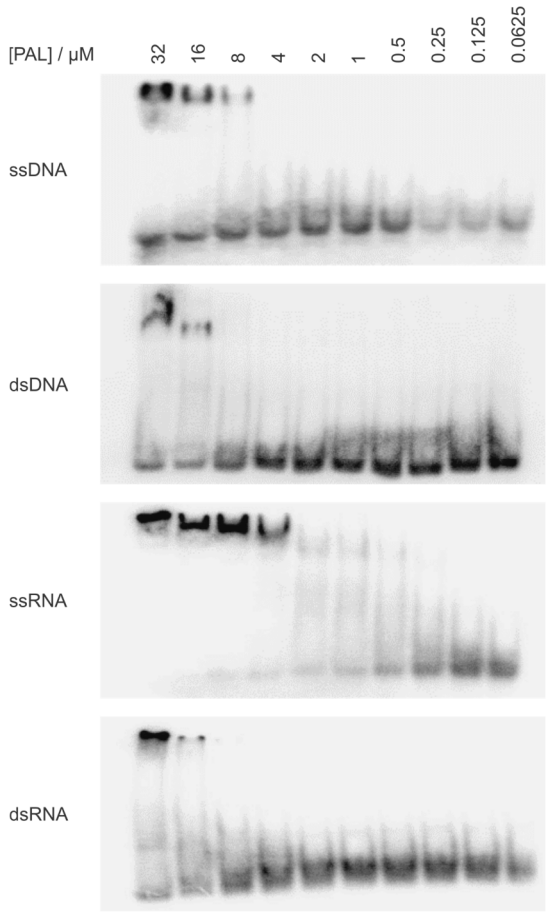


Initial characterization of PAL by electrophoretic mobility shift assays. 50 pM radiolabeled single-stranded (ss) or double-stranded (ds) DNA or RNA oligonucleotides were incubated in darkness or under blue light with decreasing concentrations of PAL (from left to right 32, 16, 8, 4, 2, 1, 0.5, 0.25, 0.125, 0.0625 µM). Reaction mixes were separated on a 6% polyacrylamide gel in Tris borate buffer and visualized by phosphorimager. Representative data of $n = 2$ biologically independent replicates are shown.

**Supplementary Figure 4**

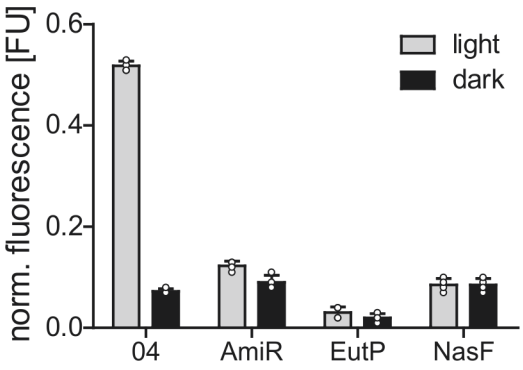


The ANTAR target sequences recognized by the *Pseudomonas aeruginosa* AmiR[55], *Enterococcus faecalis* EutV[16], and *Klebsiella oxytoca* NasR[56] proteins were analyzed for light-dependent binding to PAL via RiboGreen fluorescence in the presence of 0.5 mg $mL^{-1}$ heparin and 0.5 mg $mL^{-1}$ BSA. The PAL-specific aptamer 04 (cf. Supplementary Fig. 8) is shown for reference ($n$ = 3 biologically independent samples, mean ± SD).

**Supplementary Figure 5**

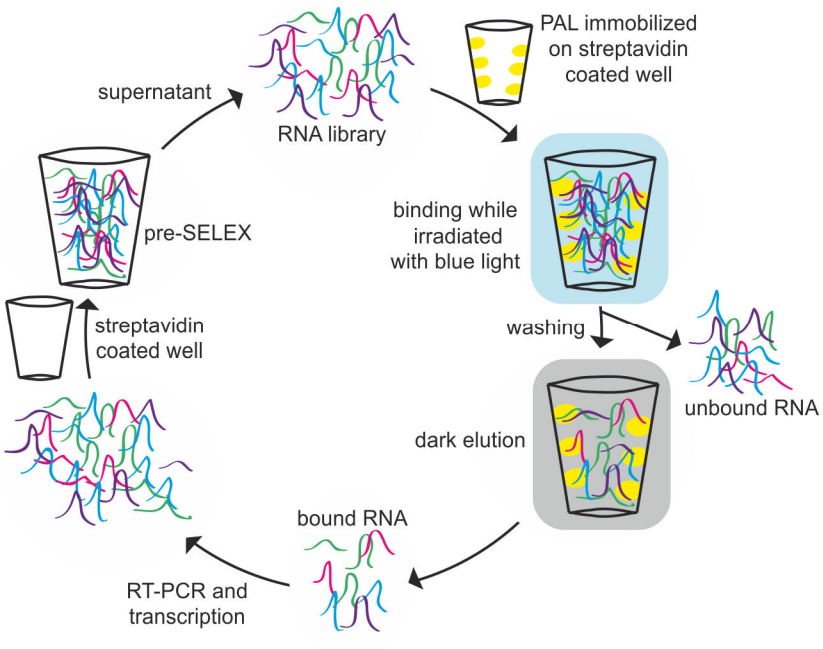


Schematic overview of the Opto-SELEX process. Biotinylated PAL is immobilized on streptavidin-coated wells and incubated with an RNA library in the presence of light. Washing steps in the light are followed by an elution step in darkness, such that predominantly those sequences elute which preferentially recognize the light-adapted conformation of PAL but not its dark-adapted conformation. Eluted sequences are reverse-transcribed, amplified by PCR and transcribed for the next cycle. Beginning with the second cycle, a pre-selection step with empty streptavidin coated wells is performed.

## Supplementary Figure 6

**a**

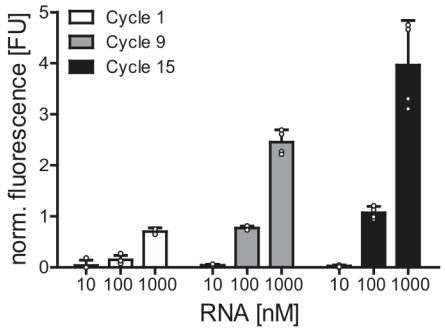


**b** **Motif 1 cycle 9 Sanger sequencing**

```
GGGAGGACGAUGCGG  GGGCAGCATGTGTCGTTCCTTCGCGTCCGGCGGGTTGAAG      CAGACGACUCGCUGAGGAUCCGAGA
GGGAGGACGAUGCGG    CCCCCCTTCAGGCTTCCTAAGTACTTTGGCGGGTTGAAG    CAGACGACUCGCUGAGGAUCCGAGA
GGGAGGACGAUGCGG CGCTCGCCTCTCCACGTTTCTCCTCGGTCACAGGGTTGAAG     CAGACGACUCGCUGAGGAUCCGAGA
GGGAGGACGAUGCGG TCCGAATGTCCTGTCTCGATTCGTCCCAGATCGAGTTGAAG     CAGACGACUCGCUGAGGAUCCGAGA
GGGAGGACGAUGCGG  AGGGCAACCGCTTGTAGACCACTCGGCTGACGAGTTGAAG     CAGACGACUCGCUGAGGAUCCGAGA
GGGAGGACGAUGCGG       TCCAACATTACCTCCCGGAACCGACATGAGTTGAAG     CAGACGACUCGCUGAGGAUCCGAGA
GGGAGGACGAUGCGG  ACATTACCGCGTACACTGAGCCTTCTTGGTAGAGTTGAAG     CAGACGACUCGCUGAGGAUCCGAGA
GGGAGGACGAUGCGG  TACGGTCCGGTCCATCCATTGTTCCTTAGAAGGGTTTGAG     CAGACGACUCGCUGAGGAUCCGAGA
GGGAGGACGAUGCGG  CTACCACGCACACTCTTTCAAGCGGGACAACGGGTTTGAG     CAGACGACUCGCUGAGGAUCCGAGA
GGGAGGACGAUGCGG  GATATTCCCTGCCGTACTTTGTCTTCAAGGCGTGTTTAAG     CAGACGACUCGCUGAGGAUCCGAGA
GGGAGGACGAUGCGG  TCCCCATCTTTTTCCGATCTCTGGGCTTGGCGCGTTGAAG     CAGACGACUCGCUGAGGAUCCGAGA
GGGAGGACGAUGCGG  ACCCCGGACCAAAATTCGTCGGGACTTTAGCGCGTTTAAG     CAGACGACUCGCUGAGGAUCCGAGA
GGGAGGACGAUGCGG         TCCCACCGATTCGTGTCCTGCCGGGAGTTTAAG     CAGACGACUCGCUGAGGAUCCGAGA
GGGAGGACGAUGCGG  CACGGATCAACCTCATCTTTCCCATCTTGGGGGGTTTAAG     CAGACGACUCGCUGAGGAUCCGAGA
GGGAGGACGAUGCGG  CACTGACAGCTTGTTCTTGTCGGATCTCGGTAGGTTTAAG     CAGACGACUCGCUGAGGAUCCGAGA
GGGAGGACGAUGCGG    TAGGGTCCTGCCTGTTGCGATCCTGGGCATGGTTTAAG     CAGACGACUCGCUGAGGAUCCGAGA
GGGAGGACGAUGCGG  TGGGCTTGACAGTCCTGCCCGGCCCGATGCGTAGTTTGAG     CAGACGACUCGCUGAGGAUCCGAGA
GGGAGGACGAUGCGG       CCCATCTCGCCTTTCCTTTACCGTCGTACGTTTGAGCAGC CAGACGACUCGCUGAGGAUCCGAGA
```

**c** **Motif 1 cycle 15 NGS**

```
GGGAGGACGAUGCGG    TGATCCACGGGTTACTGGTATCGCTCAGTGAGGTTGAAAC   CAGACGACUCGCUGAGGAUCCGAGA
GGGAGGACGAUGCGG  CCCGGCACTACGGTGTCGTACCGACATCAGCGGGTTTGAG    CAGACGACUCGCUGAGGAUCCGAGA
GGGAGGACGAUGCGG  TCTACGGTCATGCAACGTTCTTACCCTCAGTGTGTTGAAG    CAGACGACUCGCUGAGGAUCCGAGA
GGGAGGACGAUGCGG  CCCCGGTCTACGGATGGGACCCATTTTCAGCAAGTTGAAG    CAGACGACUCGCUGAGGAUCCGAGA
GGGAGGACGAUGCGG  TTCCGGTCTACGGTCTGGGCCTCTAGTCAGTGAGTTTGAG    CAGACGACUCGCUGAGGAUCCGAGA
GGGAGGACGAUGCGG  GCTCTACGGGGCTTCCCTCGACTAACTCAGCTAGTTTAAG    CAGACGACUCGCUGAGGAUCCGAGA
GGGAGGACGAUGCGG  CCAGCTCCACGGGGCCTTGCCAGCACTCAGCGGGTTTGAG    CAGACGACUCGCUGAGGAUCCGAGA
GGGAGGACGAUGCGG  CTCTCTCCACGGTCGGAGCTGCATTCGAAGTGAGTTTGAG    CAGACGACUCGCUGAGGAUCCGAGA
GGGAGGACGAUGCGG  CACATTCTACGGGACCTACCCGCATCTCAGGGAGTTTGAA    CAGACGACUCGCUGAGGAUCCGAGA
GGGAGGACGAUGCGG    TGCCCACGGTCACTTCGTCGGCGATCAGCGTGTTGGAAC   CAGACGACUCGCUGAGGAUCCGAGA
GGGAGGACGAUGCGG    TGCCTACGGTCACTTCGTCGGCGATCAGCGTGTTGGAAC   CAGACGACUCGCUGAGGAUCCGAGA
GGGAGGACGAUGCGG  CTCGGGCTACGGCTTGGTCCGCCTTGACAGCGGGTTTGAA    CAGACGACUCGCUGAGGAUCCGAGA
GGGAGGACGAUGCGG    CTCCACGGGGCAGTATTGTTTGCTCAGCGTGTTTGAG    CAGACGACUCGCUGAGGAUCCGAGA
GGGAGGACGAUGCGG  ACCAATCTACGGGTTACTGTTCGTTGTCAGCGAGTTTAAG    CAGACGACUCGCUGAGGAUCCGAGA
GGGAGGACGAUGCGG  TCACCTCTTCGGGGGATGTCGCATGATCAATGAGTTTAAG    CAGACGACUCGCUGAGGAUCCGAGA
GGGAGGACGAUGCGG  ACACATCTACGGACGTGACGTATCTTTCAGCGGGTTTAAG    CAGACGACUCGCUGAGGAUCCGAGA
```

**d** **Motif 2 cycle 15 NGS**

```
GGGAGGACGAUGCGG      TACAGCAGCGTTGCCAAAAAACGTCCACCTCAGGGATTGT  CAGACGACUCGCUGAGGAUCCGAGA
GGGAGGACGAUGCGG CCCGTACAGCAGCGATGCGGGTCGCGTGTCCACCCCGGCT      CAGACGACUCGCUGAGGAUCCGAGA
GGGAGGACGAUGCGG      TACAGCAGCGATGCCGTAGTTCTCAGGTCGGATTCGCAAA  CAGACGACUCGCUGAGGAUCCGAGA
GGGAGGACGAUGCGG     GTTCAGAAGCGCAGCTCGTTGACCCTCCATCGGTAGTACT  CAGACGACUCGCUGAGGAUCCGAGA
GGGAGGACGAUGCGG     CTTCAGCAGCGTAGGCCACGCGTTCTCGACACGGAACACT  CAGACGACUCGCUGAGGAUCCGAGA
GGGAGGACGAUGCGG    CGTACAGCAGCGTTGCGCTTATCGCACCCCCTACTGATCC  CAGACGACUCGCUGAGGAUCCGAGA
GGGAGGACGAUGCGG   TGTTCAGCAGCGAGCACGTCGCGTCTACCCCGGTGATACT  CAGACGACUCGCUGAGGAUCCGAGA
GGGAGGACGAUGCGG     CTTCAGAAGCGCAGGCTAGTTCGTCTTCGCTCTAGGTCTT  CAGACGACUCGCUGAGGAUCCGAGA
GGGAGGACGAUGCGG      TCCAGCAGCGTGGCCAGTCATCTCCTCGTCCTTGGCGATT  CAGACGACUCGCUGAGGAUCCGAGA
GGGAGGACGAUGCGG    CCTACAGCAGCGTTGGGACCACGGCCTTTCATTGAGACCT  CAGACGACUCGCUGAGGAUCCGAGA
GGGAGGACGAUGCGG      TACAGCAGCGTTGCCGATCGAACCGCTCCCGACTGGTACT  CAGACGACUCGCUGAGGAUCCGAGA
GGGAGGACGAUGCGG     CTACAGCAGCGTTGGCTGTACGATCTCCACTCCTCGGATT  CAGACGACUCGCUGAGGAUCCGAGA
GGGAGGACGAUGCGG     CTTCAGCAGCGCAGGCCGAGTGTCTTCTACATCCGTACCT  CAGACGACUCGCUGAGGAUCCGAGA
GGGAGGACGAUGCGG     CTTCAGCAGCGAGGCAAAGTCATGGTCCTACGAAGTTCCT  CAGACGACUCGCUGAGGAUCCGAGA
GGGAGGACGAUGCGG     GTTCAGCAGCGAAGCCTGGACGTCCCCCGATCGTGTCCCT  CAGACGACUCGCUGAGGAUCCGAGA
GGGAGGACGAUGCGG      TTCAGAAGCGTAGCCGCACGTTTCGCCCCCTTGGTGCT   CAGACGACUCGCUGAGGAUCCGAGA
```

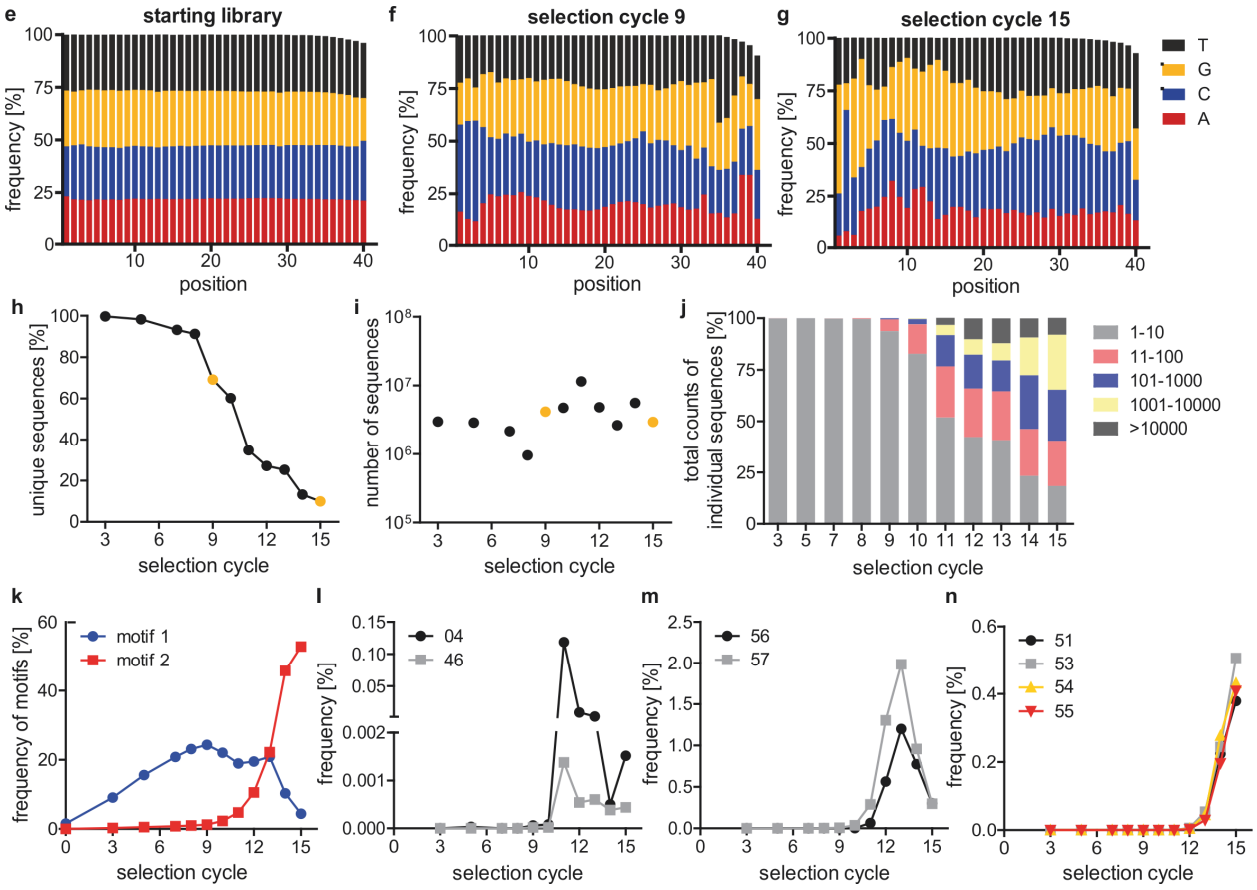


Sequence and binding analyses of aptamers from SELEX. **a**, RNA pools of SELEX cycles 1, 9 and 15 were analyzed by a fluorescence-based binding assay. Biotinylated PAL was immobilized on streptavidin-coated wells, and bound RNA was quantified by RiboGreen fluorescence. Data represent mean ± SD of *n* =3 biologically independent samples. **b-d**, Representative clones from selection cycles 9 (panel **b**) of 15 (panels **c, d**) that bear motifs 1 (panels **b, c**) or 2 (panel **d**). Sequences were determined by Sanger or next-generation sequencing as indicated. **e-g**, Nucleotide distribution of the random region at the different positions in the starting library (panel **e**), selection cycle 9 (panel **f**) and selection cycle 15 (panel **g**). **h**, Frequency of unique sequences in all analyzed selection cycles. **i**, Number of analyzed sequences in next-generation sequencing analysis. **j**, Distribution of all sequences according to indicated copy numbers in the total population of each selection cycle. **k**, Frequency of motifs 1 and 2 in all analyzed selection cycles. **l-n**, Frequency of

individual sequences in all analyzed selection cycles, where sequences 04, 46, 56 and 57 bear motif 1, and 51, 53, 54 and 55 bear motif 2 (cf. Supplementary Table 1).

**Supplementary Figure 7**

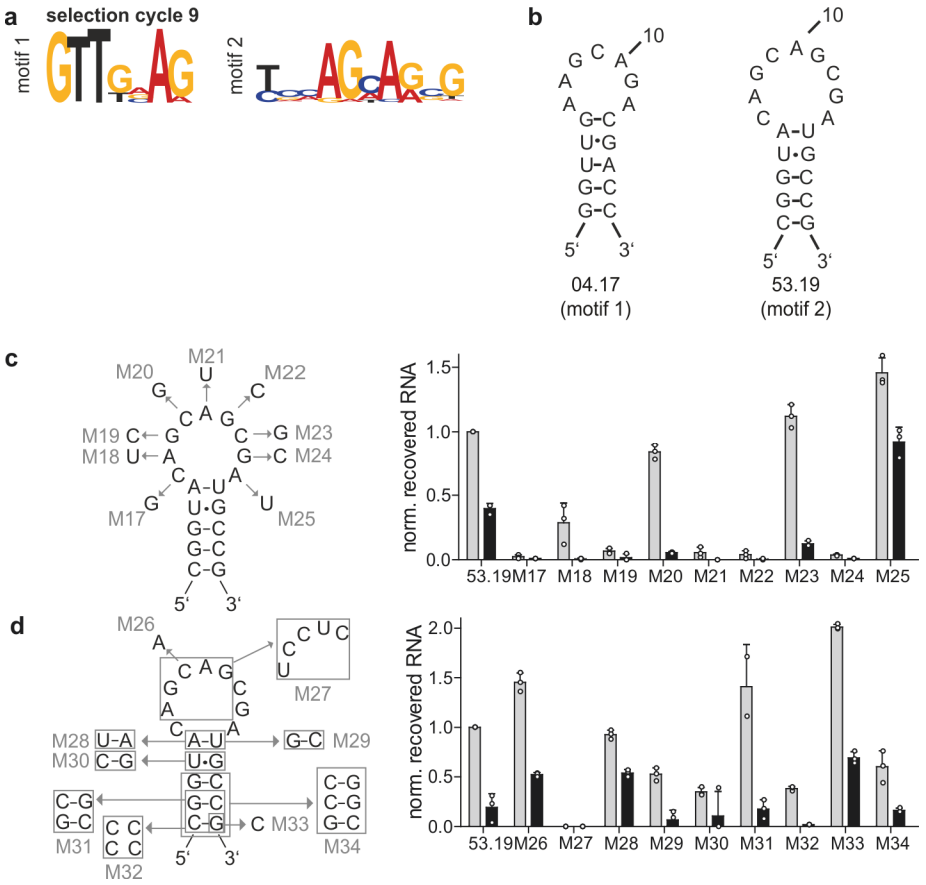


Photoactivated RNA-binding by the light-oxygen-voltage receptor PAL (Uniprot C8XJT7). **a**, Next-generation sequencing analysis identifies two PAL-binding motifs dominating in SELEX cycle 9. **b**, Sequence and predicted structure of the truncated PAL-binding aptamers 04.17 (motif 1) and 53.19 (motif 2). **c, d**, Impact of residue exchanges within the unpaired loop and the base-paired stem of the 53.19 aptamer. Data represent mean ± SD of $n$ = 3 biologically independent samples.

## Supplementary Figure 8

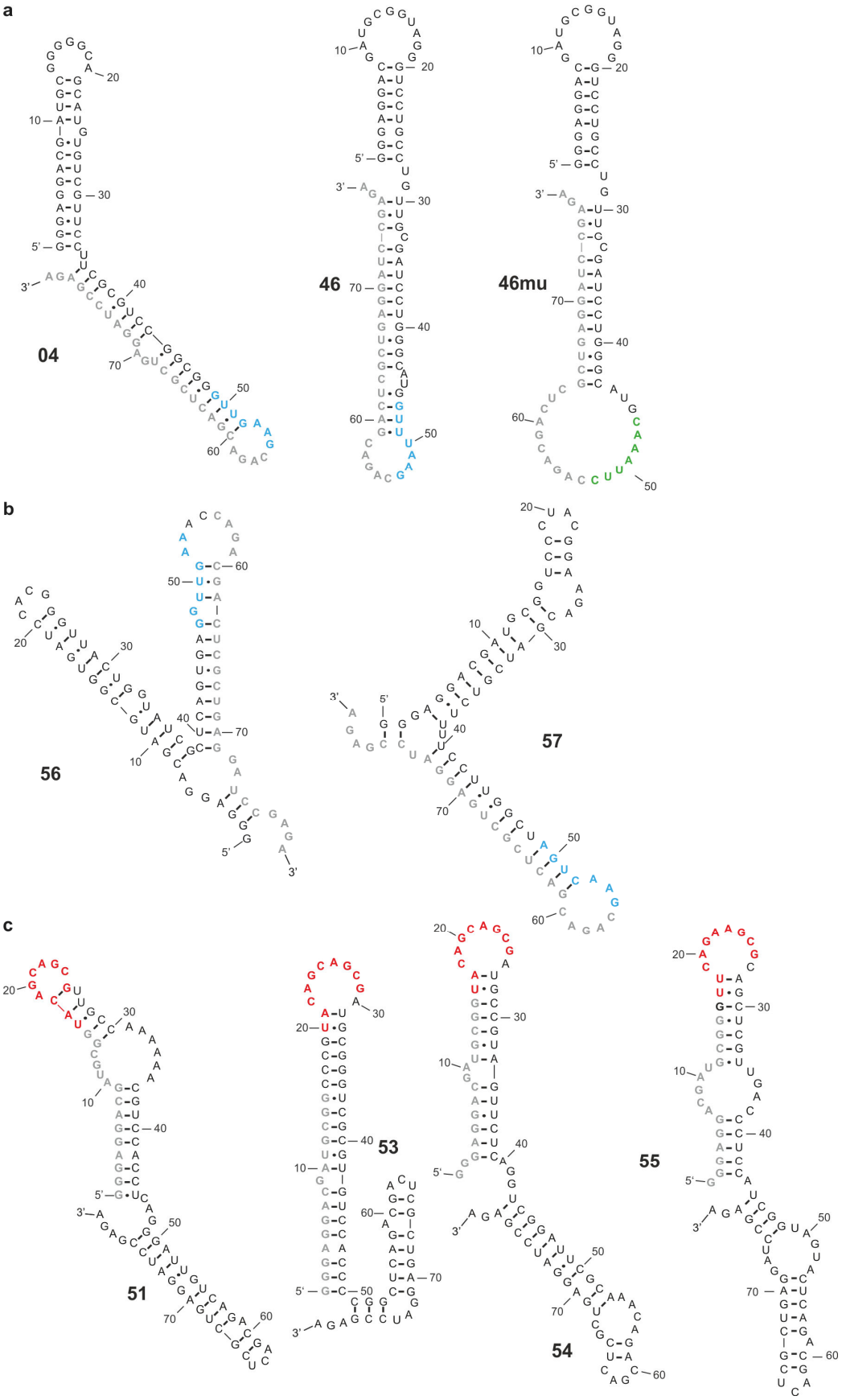

Sequence and secondary structure of aptamers from SELEX. **a-b**, Sequences and predicted secondary structure of PAL-binding aptamers of motif 1 (panels **a, b**) and motif 2 (panel **c**), obtained by Sanger (panel **a**) or next-generation sequencing (panels **b, c**). Nucleotides highlighted in blue: motif 1; in red: motif 2, in green: non-binding version of aptamer sequence in variant 46mu: in grey: location of forward and reverse primer.

**Supplementary Figure 9**

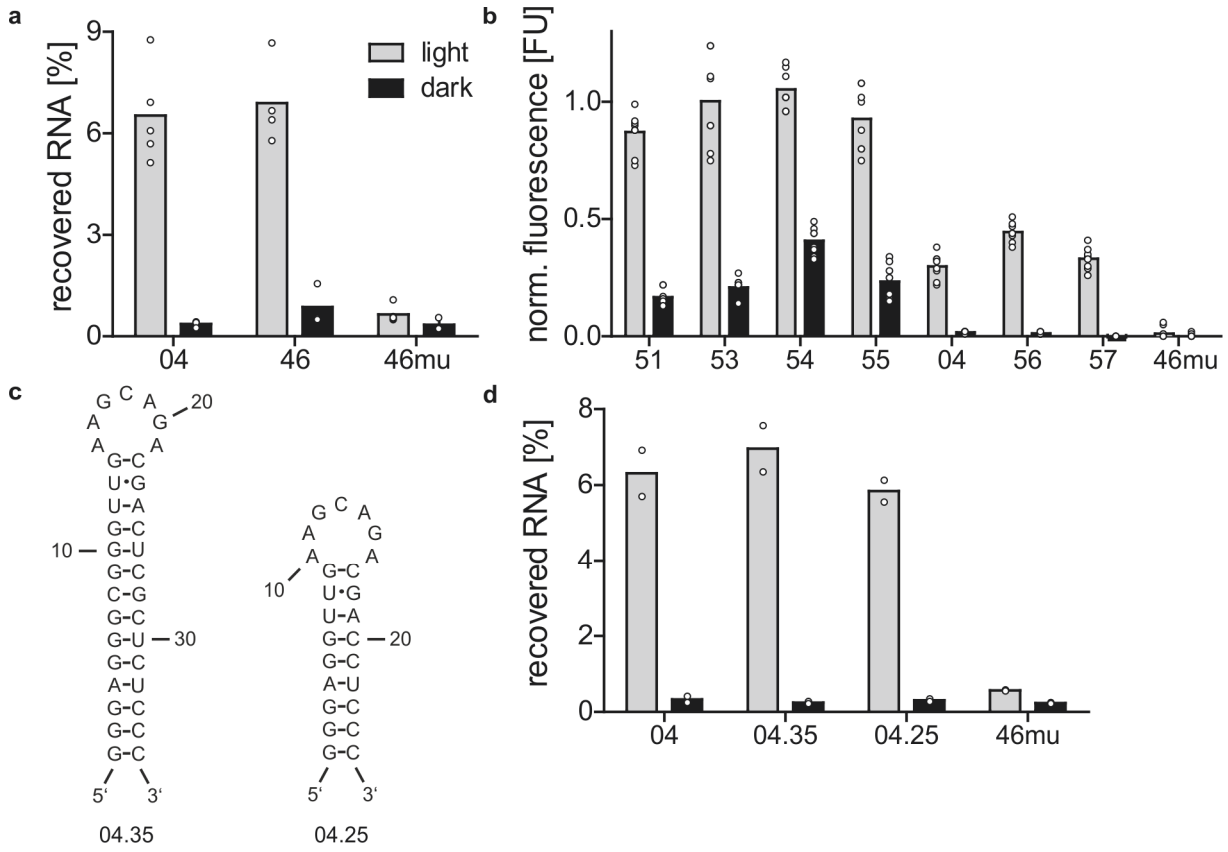


Binding analyses of aptamers from SELEX. **a**, $^{32}$P-labeled aptamers 04 and 46, and the control 46mu were analyzed for light-dependent binding of PAL immobilized on streptavidin-coated wells (mean of $n = 2$ biologically independent replicates). **b**, The aptamers 51, 53, 54, 55, 56, 57 and 04, and the control 46mu were analyzed for light-dependent binding by fluorescence. Biotinylated PAL was immobilized on streptavidin-coated wells, and binding of RNA was quantified by RiboGreen fluorescence (mean of $n = 2$ biologically independent replicates). **c**, Sequences and predicted secondary structure of truncated variants of aptamer 04. **d**, $^{32}$P-labeled aptamer 04 and truncation variants were analyzed for light-dependent binding of PAL immobilized on streptavidin-coated wells (mean of $n = 2$ biologically independent replicates).

**Supplementary Figure 10**

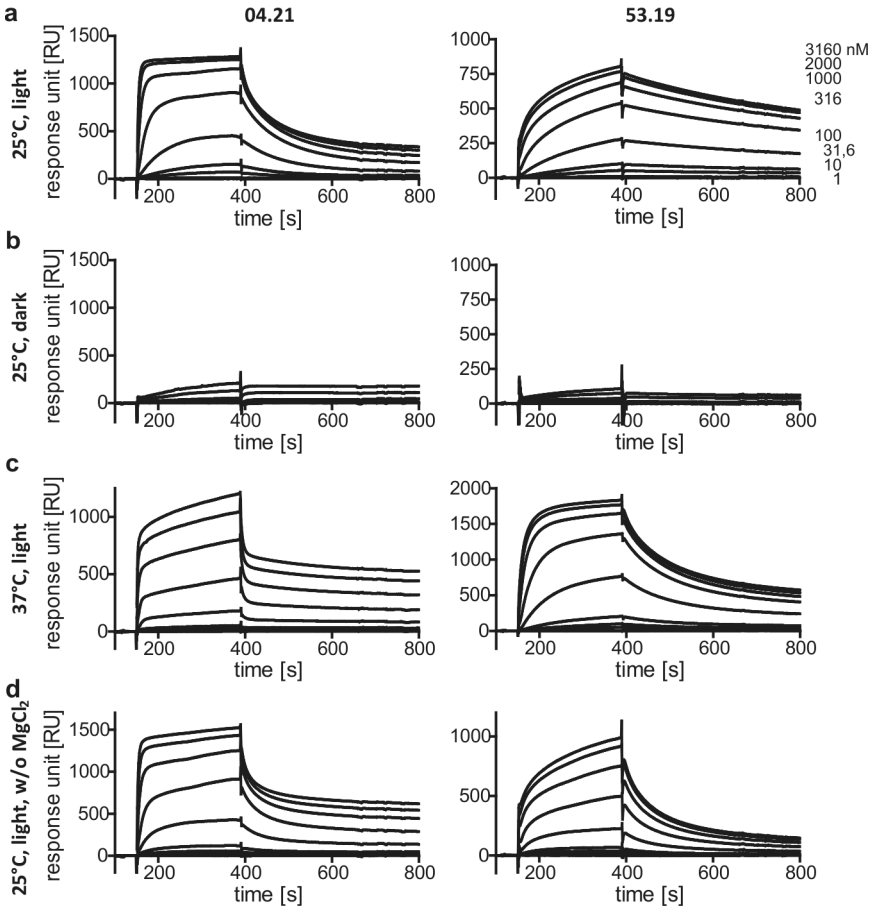


Analysis of PAL:RNA interaction by surface plasmon resonance. For the measurements, PAL at different concentration (3160, 2000, 1000, 316, 10, 31.6 10, and 1 nM) was used as analyte, and biotinylated aptamers were used as immobilized ligands. The aptamers 04.21 and 53.19 were analyzed (panel **a**) at 25°C in the presence of light, (panel **b**) at 25°C in darkness, (panel **c**) at 37°C in the presence of light, and (panel **d**) at 25°C in the presence of light and absence of $MgCl_2$. One of $n = 3$ biologically independent replicates is shown.

## Supplementary Figure 11

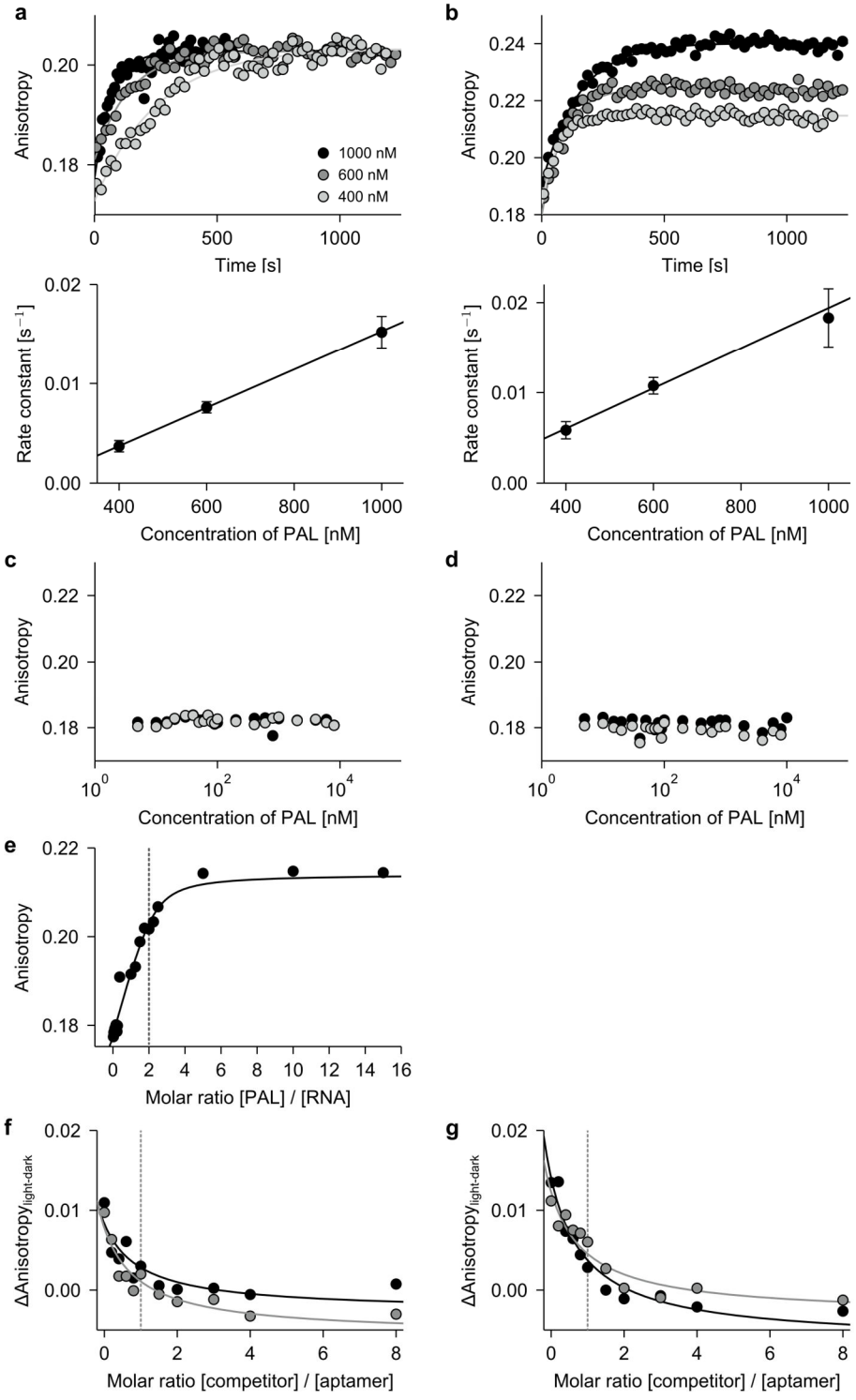

Photoactivated RNA-binding by the light-oxygen-voltage receptor PAL. **a-b**, Association kinetics of PAL with 4 nM 04.17 (panel **a**) and 53.19 RNA aptamer (panel **b**) after blue-light illumination at protein concentrations of 400 nM (light grey) 600 nM (dark grey) and 1000 nM (black) (top). The resultant pseudo-first-order rate constants are plotted against the PAL concentration to determine the bimolecular association rate constant $k_{bi}$ (bottom). **c-d**, Titration of TAMRA-labeled DNA variants of 04.17 (panel **c**) and 53.19 (panel **d**) with PAL in the dark (black circles) and following blue-light exposure (grey circles) monitored by fluorescence anisotropy. **e**, Binding isotherm recorded under blue light in the regime of stoichiometric binding at a concentration of 200 nM of the TAMRA-labeled 04.17 aptamer. Data were fitted to a single-site binding model (grey line). **f**, Competition experiments between the 04.17 and 53.19 aptamers. TAMRA-labeled 04.17 aptamer was incubated under blue light with $PAL_L$ and increasing concentrations of unlabeled, competitor aptamer 04.17 (grey circles) or 53.19 (black cirlces). Resultant isotherms were evaluated (lines) to a model where the two aptamers compete for a single binding site with equal affinity. The vertical dotted line denotes a 1:1 ratio of the two aptamers. **g**, As panel **f** but TAMRA-labelled 53.19 aptamer was incubated with unlabeled 04.17 (black circles) or 53.19 (grey circles) aptamer. Representative data of $n = 2$ biologically independent replicates are shown.

## Supplementary Figure 12

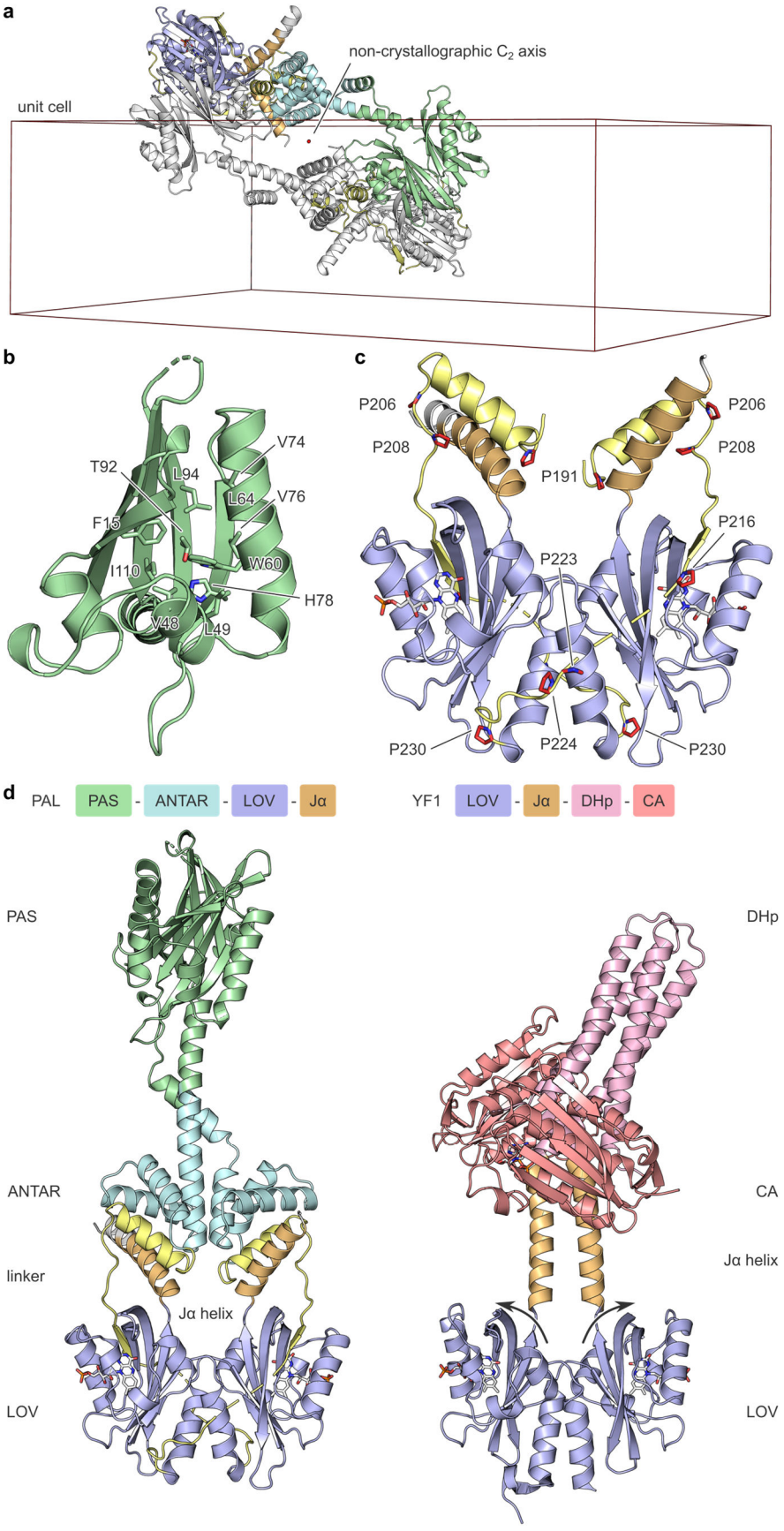

Three-dimensional structure of PAL at 2.5 Å resolution. **a**, The asymmetric unit of the crystal contains two copies of the PAL homodimer that are related by a non-crystallographic $C_2$ axis (red dot). Both dimer copies have similar environment and intermolecular contacts within the crystal lattice. **b**, The core of the PAS domain of PAL is formed by several mostly hydrophobic residues that are in van-der-Waals contact. No void cavities are present. **c**, The ANTAR and LOV domains are connected by an adapter sequence (yellow) that comprises an α helix and a long, proline-rich linker. The linker associates with strand Gβ of the LOV domain and thereby extends the antiparallel β sheet by a sixth strand. **d**, Comparison between PAL and the blue-light-repressed LOV histidine kinase YF1[22,23]. Despite different domain topology the structural arrangement of the LOV photosensor domains in the homodimeric receptors is remarkably similar. Note that in PAL the effector domain is situated N-terminally of the LOV module but YF1 realizes the more common, opposite arrangement.

**Supplementary Figure 13**

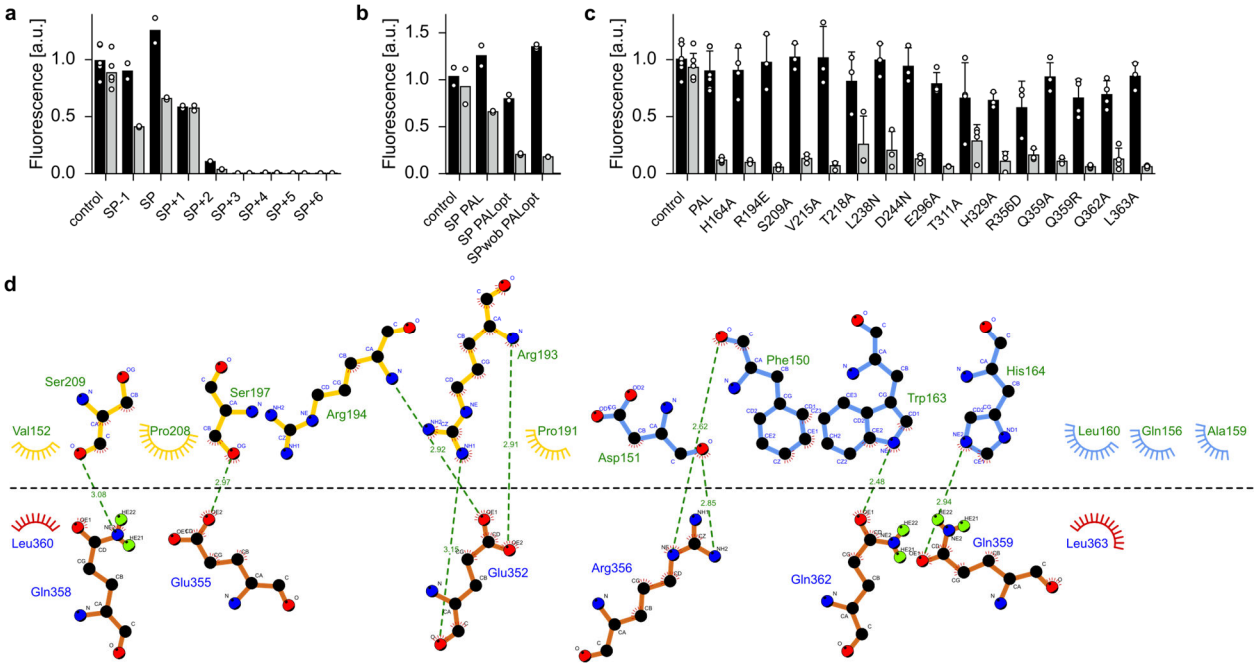


Functional analysis of PAL. **a**, Analysis of reporter constructs with a derivative of the 04.17 aptamer (lacking the wobble pair at position 4 of the stem) inserted at several positions relative to the SD sequence. Three variants with light-dependent reporter fluorescence were selected for further optimization. Data in panels **a** and **b** represent the mean of $n \geq 2$ biologically independent replicates. **b**, The introduction of a PAL variant codon-optimized for *E. coli* increased dynamic range of the reporter assay, as did the introduction of a U-G Wobble pair at position 4 of the aptamer stem. In further experiments, this aptamer, corresponding to the 04.17 aptamer, was used in combination with codon-optimized PAL. **c**, Diverse residue exchanges probed in PAL with no or small effect on light-regulated reporter fluorescence. Data represent the mean ± SD of $n \geq 3$ biologically independent replicates. **d**, Schematic of the interface which the Jα helix forms with the ANTAR α2 and adapter helices. Residues above the dashed line are located in the α2 (blue) or the adapter helix (gold), and residues below the line (tan) in the Jα helix. The plot was prepared with LIGPLOT[57].

## Supplementary Figure 14

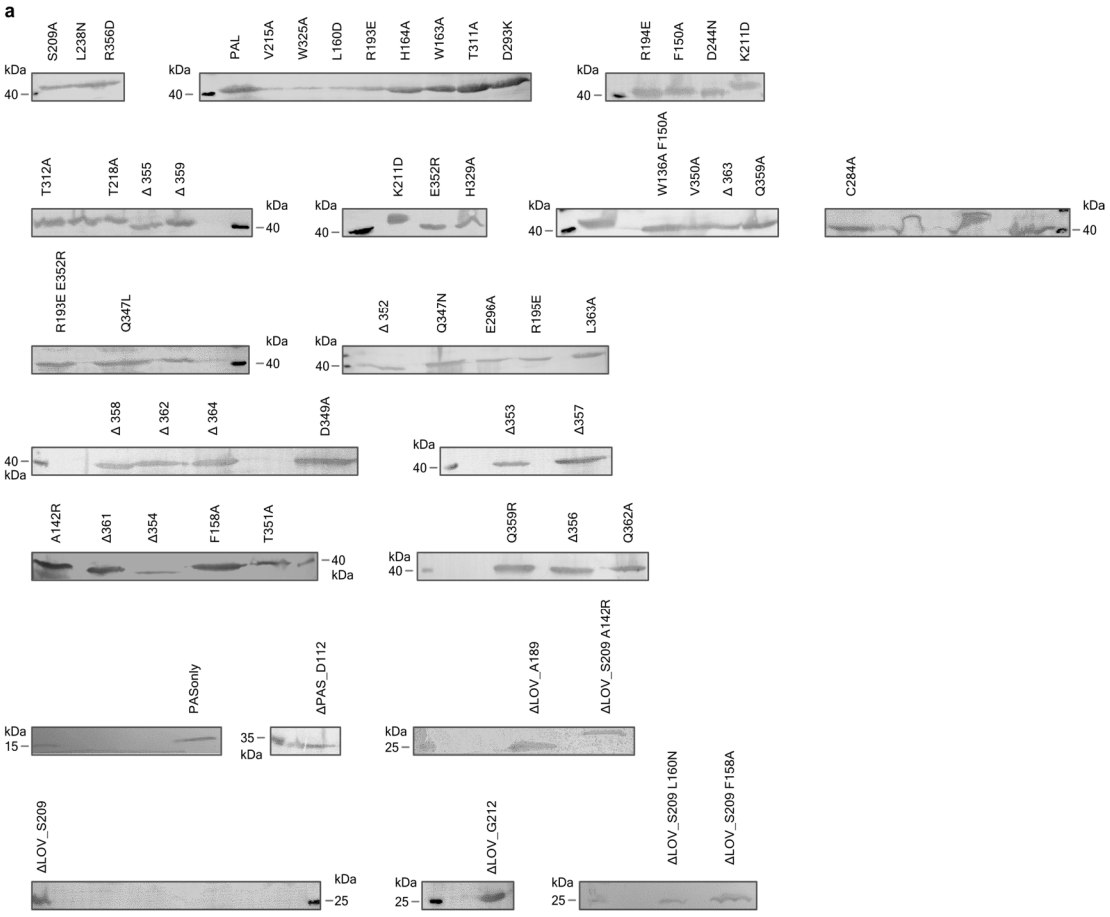

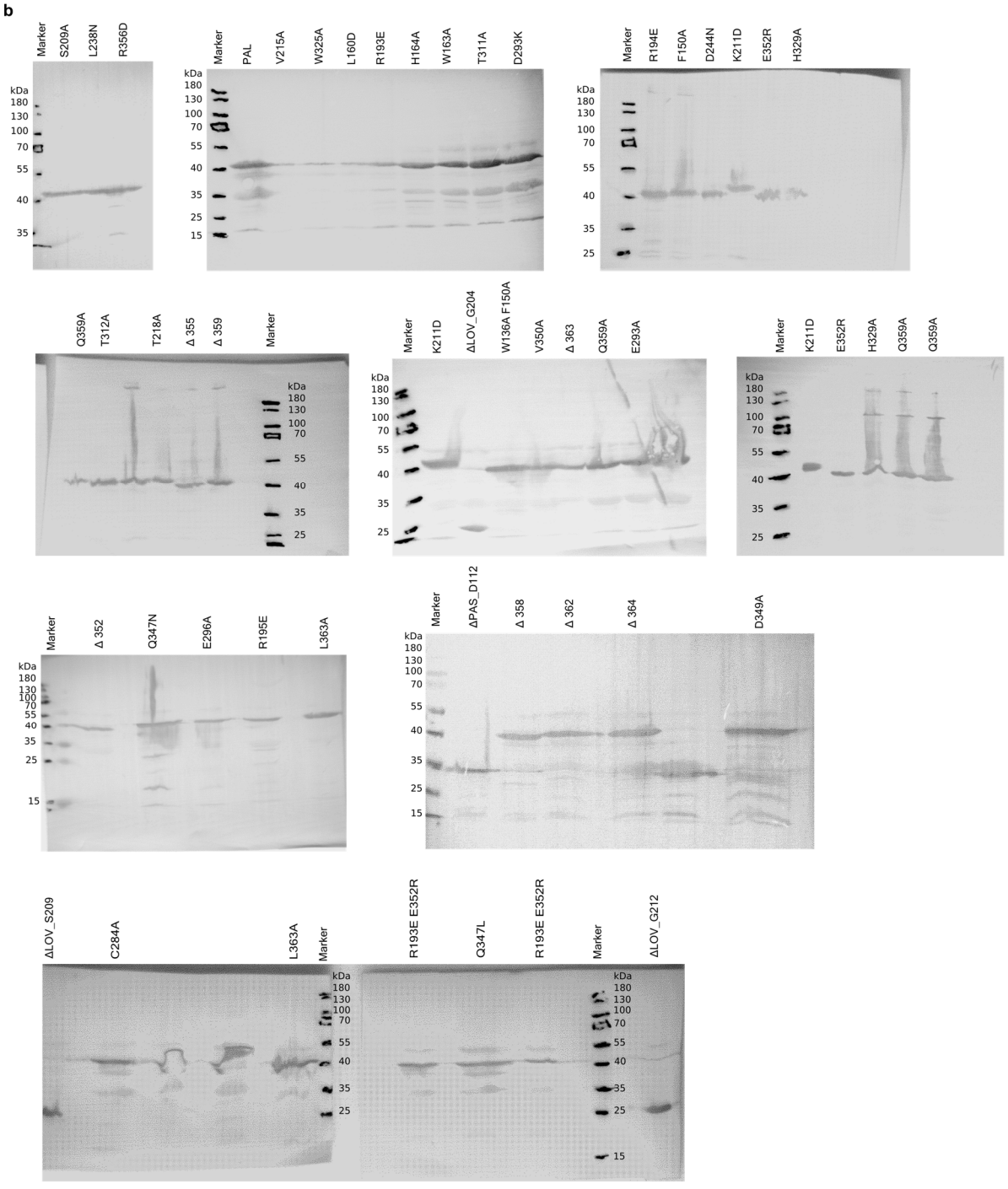
b
Marker
S209A
L238N
R356D
kDa
180
130
100
70
55
40
35
Marker
PAL
V215A
W325A
L160D
R193E
H164A
W163A
T311A
D293K
kDa
180
130
100
70
55
40
35
25
15
Marker
R194E
F150A
D244N
K211D
E352R
H329A
kDa
180
130
100
70
55
40
35
25
Q359A
T312A
T218A
Δ 355
Δ 359
Marker
kDa
180
130
100
70
55
40
35
25
Marker
K211D
ΔLOV_G204
W136A F150A
V350A
Δ 363
Q359A
E293A
kDa
180
130
100
70
55
40
35
25
Marker
K211D
E352R
H329A
Q359A
Q359A
kDa
180
130
100
70
55
40
35
25
Marker
Δ 352
Q347N
E296A
R195E
L363A
kDa
180
130
100
70
55
40
35
25
15
Marker
ΔPAS_D112
Δ 358
Δ 362
Δ 364
D349A
kDa
180
130
100
70
55
40
35
25
15
ΔLOV_S209
C284A
L363A
Marker
kDa
180
130
100
70
55
40
35
25
R1193E E352R
Q347L
R1193E E352R
Marker
ΔLOV_G212
kDa
180
130
100
70
55
40
35
25
15

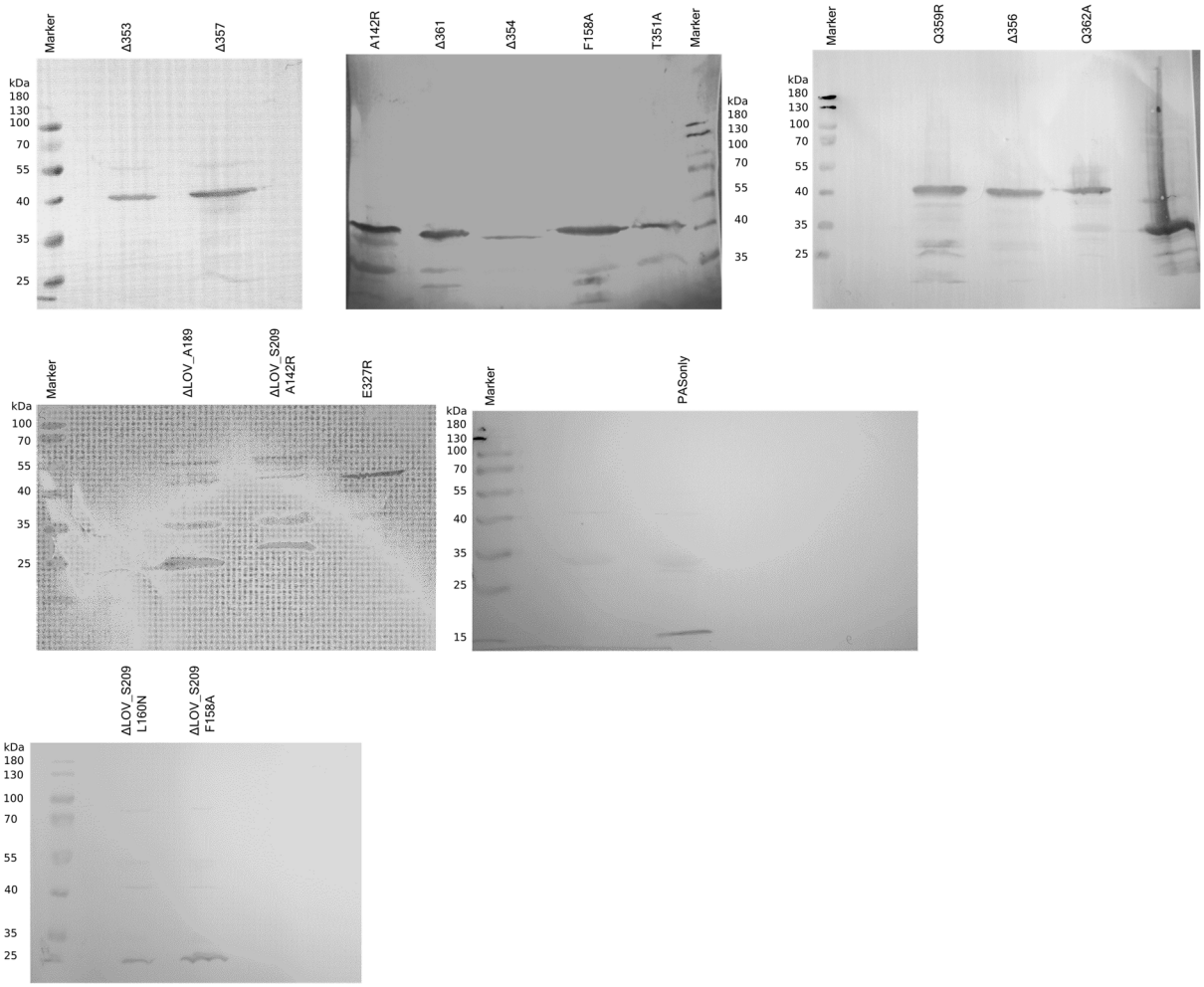


Expression analysis of PAL variants in the context of the bacterial fluorescence reporter assay (cf. Fig. 3 and Supplementary Fig. 13) via Western blot against a *myc*-tag appended to the C-terminus of the PAL variants. **a**, Cropped images. **b**, Uncropped images.

## Supplementary Figure 15

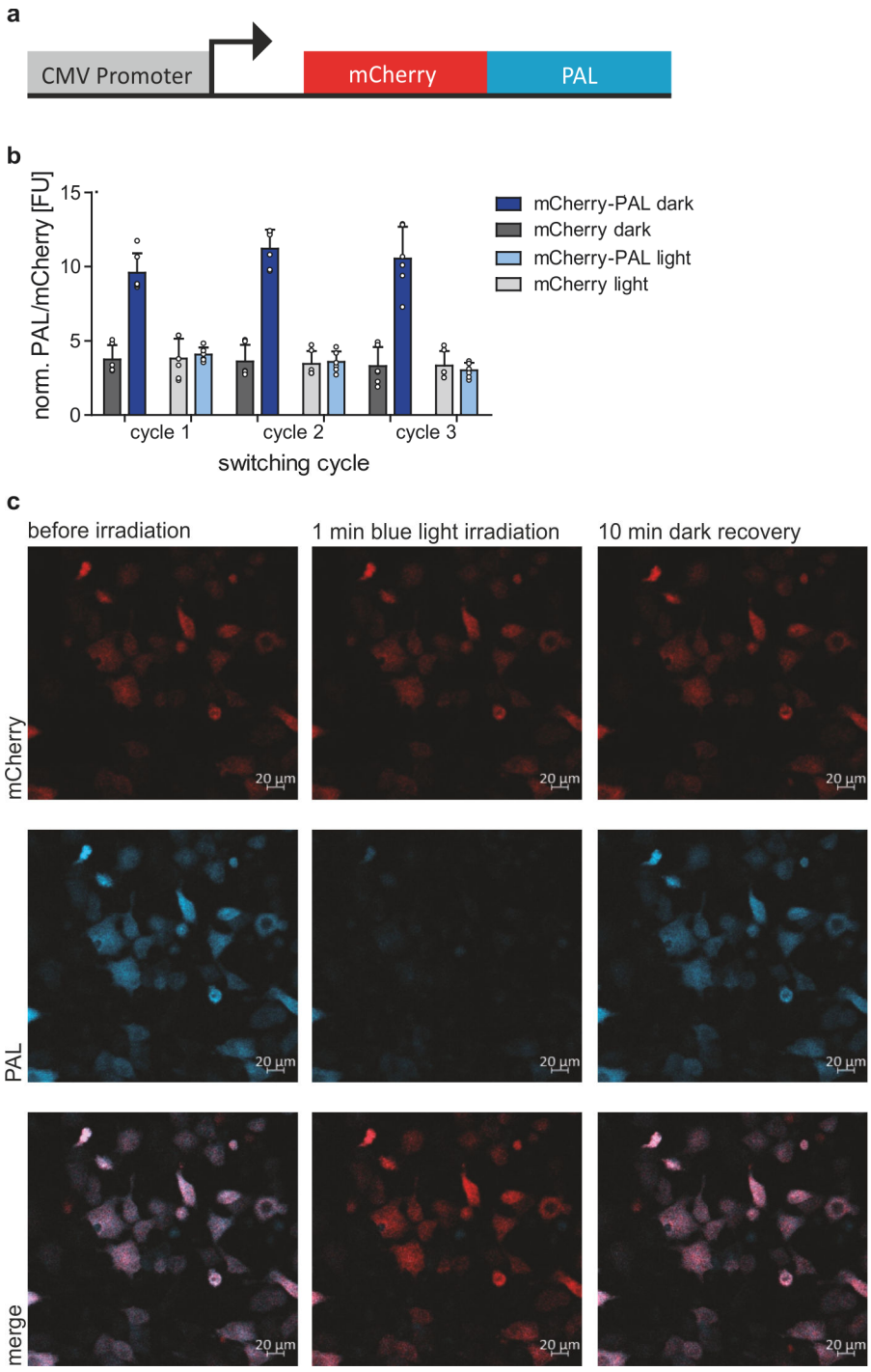


Photoswitching of mCherry-PAL in HeLa cells. **a**, Schematic of the mCherry-PAL construct used for cellular studies. **b**, Photoswitching of PAL from its dark-adapted state to its light-adapted

state reduced flavin fluorescence from the FMN chromophore to background level. Recovery of fluorescence was detected 30 min after irradiation. Fluorescence of mCherry showed no photobleaching ($n$ = 5 biologically independent samples, mean ± SD). **c**, Photoswitching analysis of PAL by laser-scanning microscopy shows the absence of a fluorescent signal after blue-light irradiation and the recovery after incubation in darkness for 10 min (ex / em: 405 nm / 488-529 nm).

## Supplementary Figure 16


Light-dependent regulation of translation in mammalian cells. Position and sequence of 53.19 aptamer variants embedded in the 5'-UTR. The entries UTRa5 and UTRa8 refer to variants that employ derivatives of the 04.17 aptamer rather than 53.19.

## Supplementary Figure 17

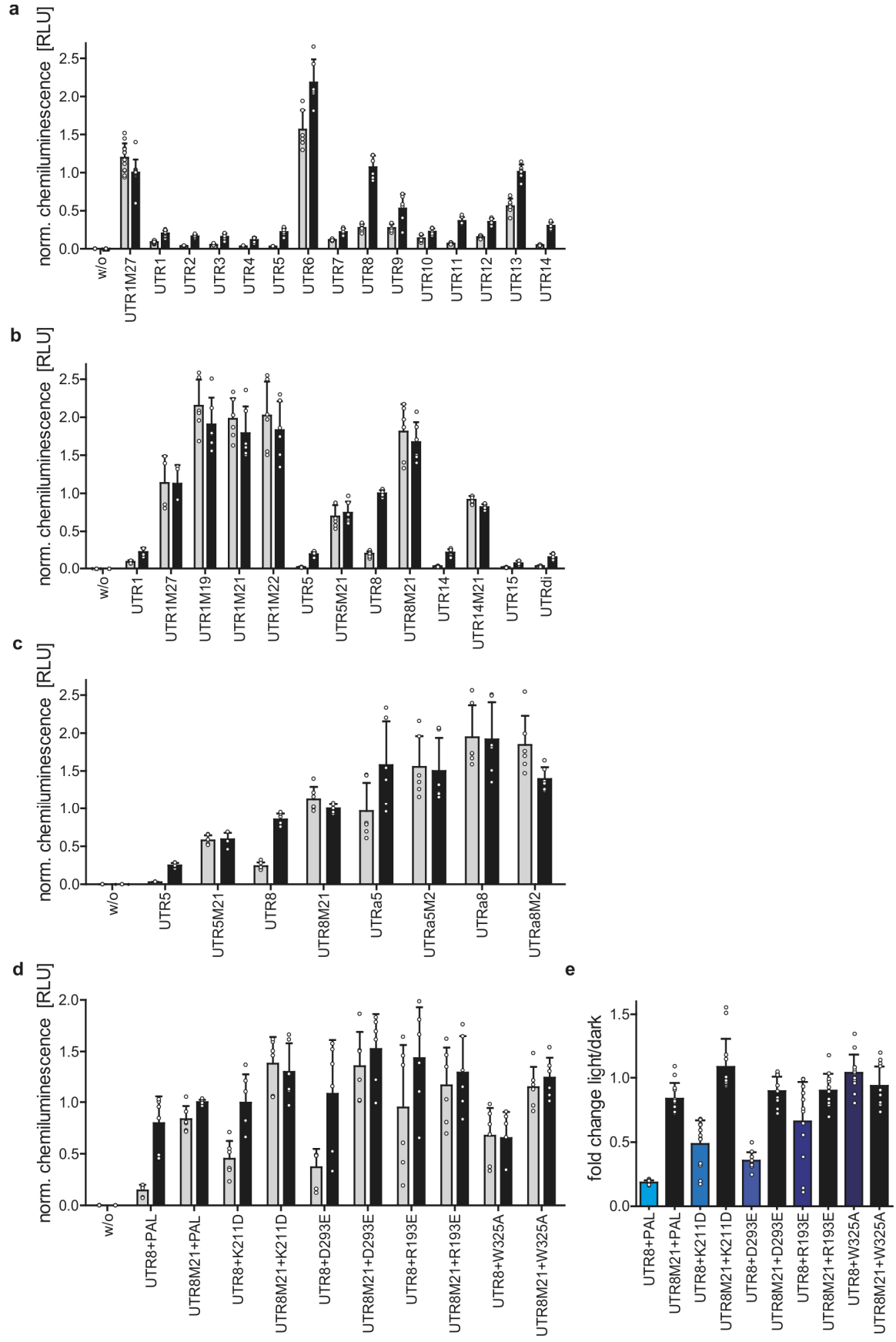

Light-dependent regulation of translation in mammalian cells. Light-induced binding of PAL to the 04.17 or 53.19 aptamers embedded in the 5'-untranslated region (5'-UTR) of an mRNA attenuates expression of a Metridia luciferase reporter in HeLa cells. **a-b**, Reporter luminescence for different 53.19 aptamers in darkness (black bars) and under blue light (grey bars) ($n$ = 3 biologically independent samples, mean ± SD). UTR variants M19-M21 and M27 harbor one or several nucleotide exchanges in the aptamer loop that abolish light responsiveness. **c**, Position and sequence of 04.17 aptamer variants embedded in the 5'-UTR. **d**, Reporter luminescence under blue light and in darkness for PAL variants bearing single-residue exchanges. **e**, Quotient of reporter luminescence under blue light and in darkness for variants from panel **d**.

**Supplementary Figure 18**

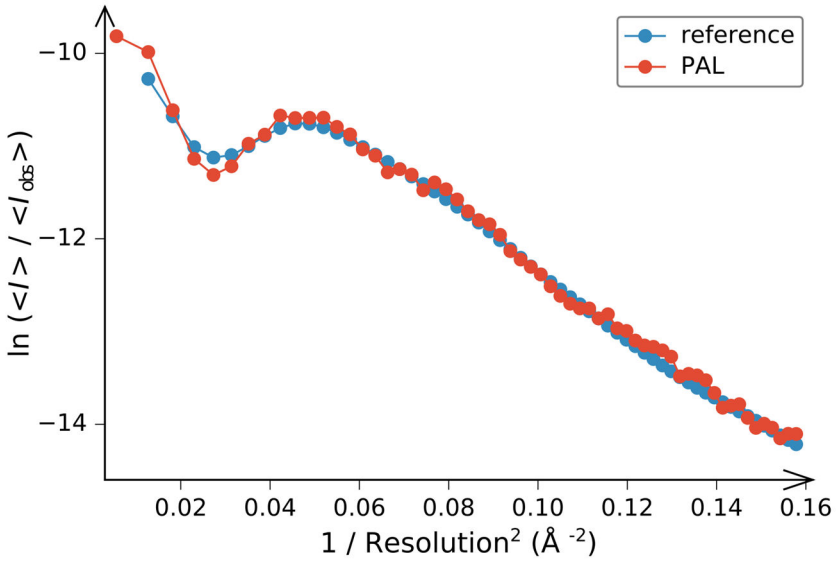


Wilson plot of the PAL native dataset at 2.51 Å resolution as calculated by POINTLESS[38]. The Wilson plot shows the drop of the mean intensity of the diffraction data with resolution in the PAL native dataset (red). The reference data (blue) are based upon an analysis of high-resolution datasets in the Protein Data Bank.

**Supplementary Dataset 1. Individual RNA Sequences from SELEX selection.**

This dataset shows the progression and enrichment of individual RNA sequences through the SELEX selection cycles 3-15, as determined by RNA sequencing.

**Supplementary References**


55. Wilson, S. A., Wachira, S. J., Norman, R. A., Pearl, L. H. & Drew, R. E. Transcription antitermination regulation of the *Pseudomonas aeruginosa* amidase operon. *EMBO J* **15**, 5907–5916 (1996).
56. Chai, W. & Stewart, V. NasR, a novel RNA-binding protein, mediates nitrate-responsive transcription antitermination of the *Klebsiella oxytoca* m5al nasF operon leader *in Vitro*. *J Mol Biol* **283**, 339–351 (1998).
57. Wallace, A. C., Laskowski, R. A. & Thornton, J. M. LIGPLOT: a program to generate schematic diagrams of protein-ligand interactions. *Protein Eng* **8**, 127–34 (1995).